

https://doi.org/10.70917/jcc-2025-020 Article

A High-Sensitivity Gas Sensor for Simultaneous Detection of Methane and Ethane in Urban Gas Networks

Zhao Rao ¹, Bin Zhou ^{1,*}, Denghao Zhu ¹, Xiao Chen ², Jingjing Liu ² and Yuan Lv ²

- ¹ School of Energy and Environment, Southeast University, Nanjing 211189, China; raozhao@seu.edu.cn (Z.R.)
- ² Technology Innovation Center of Safety Operations and Maintenance for Oil and Gas Storage and Transportation Equipment Facilities for Jiangsu Province Market Regulation, Nanjing 210009, China
- * Correspondence author: zhoubinde@seu.edu.cn

Abstract: To address the challenge of precise discrimination of multi-component trace gases for urban natural gas leakage monitoring, a dual-component gas sensor based on mid-infrared laser absorption spectroscopy was developed for simultaneous detection of methane (CH₄) and ethane (C₂H₆). The sensor integrates an interband cascade laser, a 13-m optical path length multi-pass gas cell and a high-sensitivity detector. The optimal absorption lines of CH₄ and C₂H₆ were identified through analysis of gas absorption spectra, and the negative-pressure (0.24 atm) operation was applied to effectively suppress water vapor interference, which significantly improved the anti-cross-interference capability. Experimental results demonstrate minimum detection limits of 17.77 parts-per-billion in volume (ppbv) for CH₄ and 12.95 ppbv for C₂H₆ at a 1-second averaging time, and the dynamic response time is approximately 6 s. During the In-vehicle mobile monitoring experiment, the changes of CH₄ and C₂H₆ concentrations near the leakage source show a high degree of correlation (Pearson correlation coefficient of 0.9991), which effectively distinguishes natural gas leakage from biogenic and anthropogenic interference sources such as landfills, automobile exhaust. This research provides a high-precision and low-false-alarm solution for the safety inspection of urban gas pipeline networks, and the application scenarios can be further expanded through miniaturization and intelligent optimization in the future.

Keywords: urban natural gas leakage; safety Inspection; dual-component gas; mid-infrared; mobile monitoring

1. Introduction

Due to the escalating global energy consumption and the ongoing adjustment of the energy mix, the proportion of natural gas in the energy structure has been increasing, consequently driving up domestic demand for natural gas (Li et al., 2019). Owing to its high calorific value, superior energy conversion efficiency, environmental friendliness, and economic practicality, natural gas is progressively emerging as a principal energy alternative for municipal infrastructure and domestic consumption in cities of varying scales (Faramawy et al., 2016). However, the persistent problem of natural gas leakage remains a significant concern in both the natural gas production and transportation sectors (Halley, 2021). Natural gas leakage not only leads to environmental pollution, resource waste and infrastructure damage, but also poses significant risks to human lives and property safety (Cho et al., 2022). Especially in the process of urbanization, with the combined impacts of transportation emissions and industrial activities, accurate monitoring of trace gases in complex environments is the especially serious challenge (Shelton et al., 2022). Recent advances in sensor fusion and machine learning have demonstrated significant potential for enhancing environmental monitoring in complex scenarios, such as healthcare facilities where integrating multi-source data improves prediction accuracy (Rosli Razak et al., 2025). With the widespread adoption of natural gas, numerous urban gas pipeline networks are being newly constructed and operated, consequently heightening the risk of urban gas leaks (Barriault et al., 2021). Therefore, trace gas detection has garnered significant attention in natural gas leakage monitoring, with increasing



Copyright: © 2025 by the authors

emphasis on detecting methane and ethane, which are the primary components of natural gas (Menduni et al., 2022).

Compared to non-optical detection techniques such as electrochemical sensing (Aldhafeeri et al., 2020), infrared absorption spectroscopy provides distinct advantages in selectivity, stability, and realtime in situ detection due to its reliance on molecular vibrational signatures, while maintaining high precision and rapid response (Jeevaretanam et al., 2023). A compact methane sensor was presented using an integrating sphere and interband cascade laser at 3313 nm (Davis et al., 2023). An in-vehicle CH₄ sensor was developed for mobile detection of natural gas leaks, utilizing a tunable diode laser operating at the 1.651 μ m CH₄ absorption line. The sensor achieved a detection sensitivity of $10 \sim 15$ ppbv under laboratory conditions, with a practical detection limit of approximately 30 ppbv during mobile field measurements (Mchale et al., 2019). A compact quartz-enhanced photoacoustic spectroscopy sensor was developed, utilizing a single interband cascade laser (ICL) source tunable around 3.3 µm, for simultaneous detection of methane (CH_4), ethane (C_2H_6), and propane (C_3H_8). By sequentially targeting their absorption lines, the sensor achieved detection limits of 90 ppbv (CH₄), 7 ppbv (C₂H₆), and 3 ppmv (C₃H₈) at a 1-s integration time (Sampaolo et al., 2019). A novel methane leak monitoring system was developed that focuses on the influence of environmental conditions on measurement results (Floridia et al., 2019). Although numerous studies have been conducted in this field, prevalent issues such as significant sensitivity discrepancies and unverified stability of synchronized detection under dynamic mobile conditions still pose challenges to meeting the practical demands for rapid, accurate, and simultaneous monitoring of multi-component trace gases in real-world scenarios like natural gas leakage.

Methane (CH₄) is the primary component of natural gas, while ethane (C_2H_6) is the second largest component of natural gas after CH₄ (Zou et al., 2022). C₂H₆ serves as a unique tracer for natural gas leaks because biogenic methane sources (e.g., landfills) or combustion emissions (e.g., vehicle exhaust) lack C₂H₆, whereas propane (C₃H₈), while present in natural gas, typically exists at trace levels (<1%) in pipeline systems. Detecting propane would require significantly higher sensitivity, which is unnecessary for distinguishing natural gas leaks from biogenic/anthropogenic methane sources. Additionally, C₃H₈ is also common in liquefied petroleum gas (LPG), further reducing its diagnostic specificity. Thus, propane's low concentration and cross-source prevalence render it unsuitable for reliable identification. The simultaneous detection of CH₄ and C₂H₆ effectively differentiates natural gas leakage from biogenic or anthropogenic interference sources by leveraging their distinct compositional signatures (Zifarelli et al., 2023). Therefore, this paper innovatively proposes a mobile dual-component synchronous detection system based on mid-infrared setup. By employing negative-pressure operation to suppress water vapor interference, the system significantly enhances the reliability and sensitivity of dual-component detection. Specifically, the dual-species detection in mobile use enables effective differentiation between natural gas leaks and other interference sources. The direction and spatial spread of CH₄ and C₂H₆ leaks were estimated through dynamic mobile monitoring during field experiments. This contributes to enhancing the accuracy of gas leakage detection, minimizing false alarms, and saving time during gas network safety inspections.

2. Sensor Design

2.1. CH₄ and C₂H₆ Absorption Lines Selection

The selection of gas molecular absorption spectral lines will directly affect the measurement accuracy, anti-interference ability, and other performance characteristics of the sensor. In this study, a mid-infrared continuous-wave interband cascade laser was employed as the light source. The absorbance characteristics of CH_4 and C_2H_6 spectral lines were systematically analyzed through numerical simulations. CH_4 and C_2H_6 exhibit strong absorption bands near 3.34 μ m. Optimal absorption lines were identified through iterative screening of the target gas absorption spectra within the laser tuning range, with their key spectral parameters tabulated in Table 1.

Table 1. The main parameters of absorption lines for CH₄ and C₂H₆.

Gas	Wavenumber	S(296K)	ζair	$\xi_{ m self}$	E''
Gas	[cm ⁻¹]	[cm ⁻² ·atm ⁻¹]	[cm ⁻¹ ·atm ⁻¹]	[cm ⁻¹ ·atm ⁻¹]	[cm ⁻¹]
	2989.033	1.5999	0.0652	0.079	62.8757
$\mathrm{CH_{4}}$	2988.932	1.5950	0.0694	0.079	62.8768
	2988.795	2.6653	0.0633	0.079	62.8781
C_2H_6	2986.705	0.4391	0.0741	0.124	59.6605

High-resolution transmission molecular absorption database (HITRAN) is a worldwide standard for calculating or simulating atmospheric molecular transmission and radiation, which covers a wide spectral

region from the microwave to the ultraviolet (Gordon et al., 2022). Absorption spectra of 2 ppmv CH₄, 100 ppbv C₂H₆, and 2% H₂O at different pressures are depicted in Figure 1. Based on the HITRAN database, the Optimal absorption lines of CH4 are located at 2989.033 cm⁻¹ (with an intensity of 6.453 \times 10⁻²⁰ cm/mol), 2988.932 cm⁻¹ (6.433 \times 10⁻²⁰ cm/mol), 2988.795 cm⁻¹ (1.075 \times 10⁻¹⁹ cm/mol). Additionally, a C_2H_6 absorption line centered at 2986.705 cm⁻¹ (intensity of 1.771 × 10^{-20} cm/mol) is selected as the optimum target line for C₂H₆ detection. At the selected absorption lines of CH₄ and C₂H₆, the primary spectral interference arises from water (H2O), which can affect the detection of CH4 and C_2H_6 . Although the intensity of the absorption line of H_2O at these wavelengths is 1.102×10^{-22} cm/mol, $2 \sim 3$ orders of magnitude smaller than those of CH₄ and C₂H₆. Under standard atmospheric pressure (1 atm), the absorption spectra of CH₄ and C₂H₆ exhibit significant cross-interference with the water absorption spectrum, resulting in a pronounced influence. However, under negative pressure (0.24 atm), the collision width decreases and the spectral width narrows. This results in a smaller and relatively flat overlap between the water absorption spectral lines and those of CH₄ and C₂H₆, making their influence negligible. Consequently, this effectively avoids interference from H₂O in the detection of CH₄ and C₂H₆. Furthermore, to prevent mirror contamination resulting from water vapor condensation in the gas cell, the working temperature should be maintained at 315 K. This temperature ensures that the internal surfaces remain above the dew point of the ambient environment, effectively suppressing condensation.

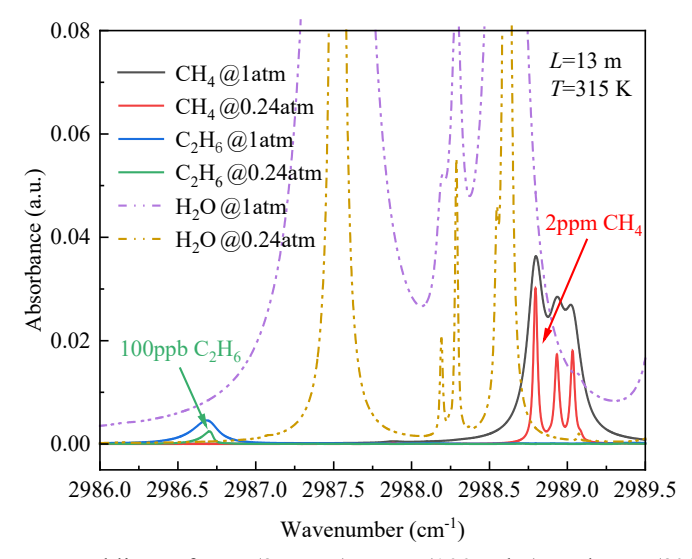


Figure 1. Absorption spectral lines of CH₄ (2 ppmv), C_2H_6 (100 ppbv), and H_2O (2%) from 2986.0 cm⁻¹ to 2989.5 cm⁻¹ under different pressures.

2.2. System Design

The schematic of the CH₄ and C₂H₆ two-component gas sensor developed based on mid-infrared laser absorption spectroscopy is shown in Figure 2. The sensor system primarily includes a mid-infrared laser, a multi-pass gas cell, mid-infrared photodetectors, and a data acquisition card. The interband cascade laser (ICL, model: Nanoplus, 3345nm) emits light across the wavenumber range of 3336 ~ 3354 cm⁻¹. The laser drive current is stabilized by a precision current controller, and its operating temperature is maintained via a thermoelectric temperature controller to ensure coverage of methane absorption lines at 2989.033cm⁻¹, 2988.932cm⁻¹, 2988.795cm⁻¹, and the ethane absorption line at 2986.705 cm⁻¹. This configuration enables simultaneous scanning of both CH₄ and C₂H₆ absorption peaks and outputs the beam at the desired wavenumbers. The output beam is split into two beams by a beam splitter mirror. One path directs the beam through an etalon to the detector. By analyzing the etalon's transmission peaks, the system measures the beam's spectral stability and calibrates its relative wavenumber position. The other beam enters a multi-pass gas cell (MPGC), achieving an effective optical path length of 13 meters through multiple internal reflections. The mid-infrared photodetector (VIGO PVI-4TE) detects the intensity of light transmitted through the MPGC and converts it into a voltage signal. The data acquisition card (NI MYDAQ) acquires the analog output signal from the detector through its built-in analog-todigital converter. The digitized signal is then processed by dedicated software to calculate the gas concentration.

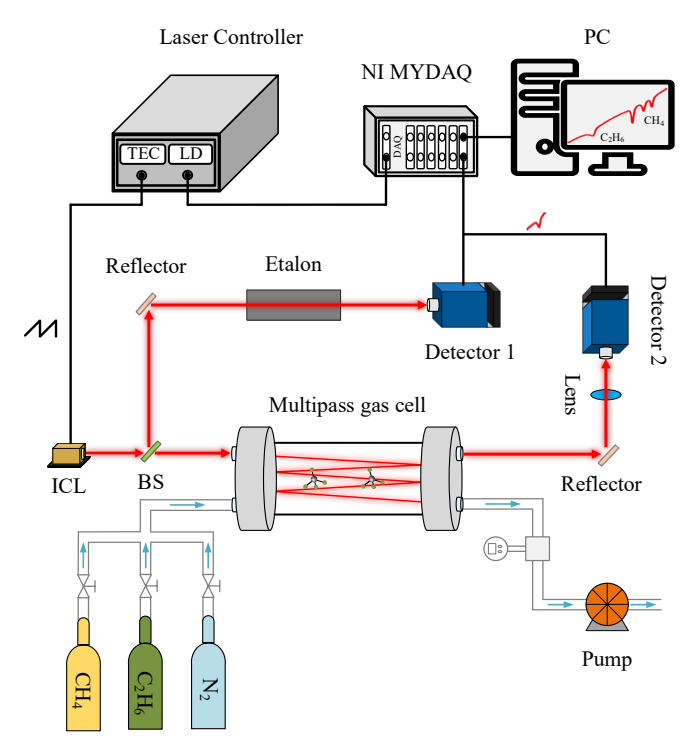


Figure 2. Schematic of the CH₄ and C₂H₆ two-component gas sensor.

3. Sensor Performance

3.1. Measurement Precision and Stability

System stability can be influenced by mechanical noise, electrical noise, and optical noise arising from environmental vibrations, electromagnetic interference, and photonic fluctuations, respectively. Allan deviation analysis was applied to evaluate the gas sensor's stability and determine its minimum detection limit (MDL) at optimal integration time. Separate measurements of 2 ppmv CH₄ and 1 ppmv C₂H₆ samples are conducted for 20 minutes continuously. Figure 3(a) exhibits the measured concentration of 2 ppmv CH₄. The results indicate that the CH₄ concentration ranges from 1.98 ppmv to 2.04 ppmv, with an average of 2.01 ppmv and a relative error of 0.5%. The Allan deviation of the CH₄ measurement is shown in Figure 3(b). The plot demonstrates that the MDL of CH₄ is 17.77 ppbv at 1 s integration time, and further decreases to the MDL of 1.19 ppbv when the integration time is extended to 326 s. This highlights the excellent detection performance of the reported sensor system.

The C_2H_6 concentrations determined from the measurements over 20 minutes are shown in Figure 4(a). The measurement results indicate that the C_2H_6 concentrations vary between 0.976 ppmv and 1.018 ppmv. The average concentration of C_2H_6 is 0.998 ppmv, with a relative error of 0.2%. The Allan deviation plot for C_2H_6 , shown in Figure 4(b), demonstrates that the MDL is approximately 12.95 ppbv with a 1 s integration time. The sensitivity of the sensor improves as the integration time increases in the noise-dominated regime. Therefore, it can achieve an MDL of 0.26 ppbv with an optimum integration time of 393 s. When the integration time exceeds the optimal duration, the Allan deviation becomes dominated by low-frequency drift, primarily caused by thermal instability of the ICL and electronic components. Improving heat dissipation in the chassis can mitigate this drift, thereby enhancing the detection limit by improving long-term stability.

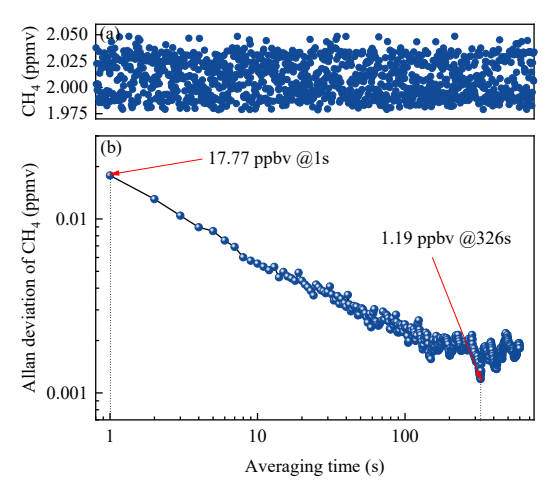


Figure 3. (a) The measured CH₄ concentrations, (b) Allan deviation analysis of CH₄.

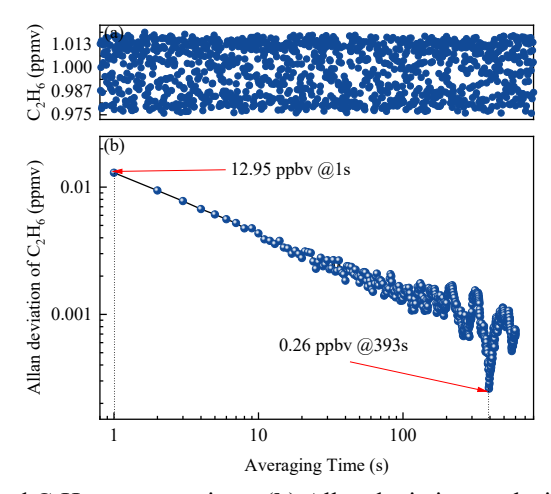


Figure 4. (a) The measured C₂H₆ concentrations, (b) Allan deviation analysis of C₂H₆.

3.2. Dynamic Measurement for Different Concentration Levels

A gas dilution system (HRHG310) was used to mix 10 ppmv CH₄ with pure nitrogen in various proportions to produce CH₄ gas mixtures of different concentrations. The output port of the gas dilution system was connected directly to MPGC, and the CH₄ gas mixture was then pumped into the MPGC using a vacuum pump (Parker D1010-22) for real-time detection. During the experiment, the gas flow rate is stabilized at 660 mL/min. The dynamic measurements for different CH₄ concentrations are shown in Figure 5. The CH₄ concentration increases stepwise from 2 to 4 ppmv, then decreases sequentially back to 2 ppmv. The CH₄ concentrations measured in the dynamic experiment were 2.05, 3.04, and 4.04 ppmv respectively. All experimental values closely match the standard reference values, with relative errors below 3%. The measurement deviation is primarily caused by systematic errors in the gas dilution system, such as inaccuracies in calibration or gas mixing ratios.

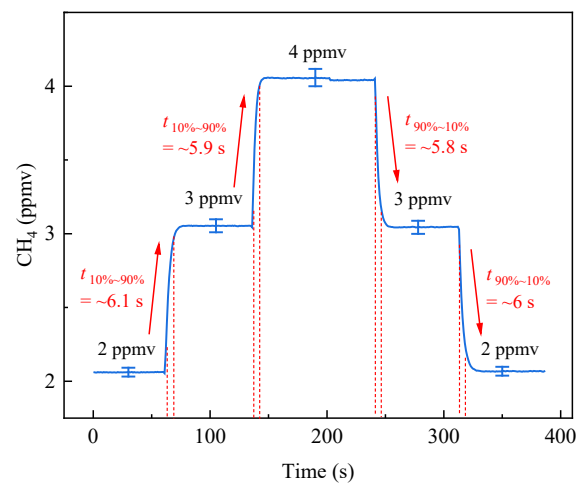


Figure 5. The measurements of different CH₄ concentration levels.

As shown in Figure 5, the sensor exhibits 10 - 90% rise times of ~ 6.1 s, ~ 5.9 s, and 90-10% fall times of ~ 5.8 s, ~ 6.0 s, respectively. The average response time of the sensor is approximately 6 s. The response time is determined by the internal volume of the MPGC, the gas flow speed through the MPGC, and the processor's processing time. It's worth noting that the reported response time includes the mixing time of the gas dilution system. When the response contribution of the gas dilution system is decoupled, the sensor's actual response time is even shorter.

The uncertainty analysis is conducted following the rules of "Guide to the expression of uncertainty in measurement" (GUM). The coverage factor, k, is given as 1 throughout the uncertainty evaluations. According to the GUM, the combined standard uncertainty u(x) is the positive squared root of the combined variance which is given by:

$$u(x) = \sqrt{\sum_{i=1}^{N} \left(\frac{\partial f}{\partial Y_i} \cdot u(Y_i)\right)^2}$$
 (1)

where $u(Y_i)$ is the uncertainty of the i_{th} quantity Y_i .

For the uncertainty of CH₄ mole fraction, the correlations between mole fraction x and related quantities Y_i can be expressed through a functional relationship:

$$x = f(A, L, p, T, v_0, S(T))$$
(2)

where L is the optical path length, S(T) is the line intensity. Once the uncertainty of each quantity is clear, the uncertainty of the CH₄ mole fraction can be calculated by equation (1). In this study, the uncertainty of CH₄ mole fraction is 1.45%.

Table 2. Uncertainty budgets of CH₄ mole fraction.

Quantity	Value	Uncertainty (%)	Index (%)
A	0.00344	1	49.1
P	0.24 bar	0.42	8.5
L	1300 cm	0.23	2.6
T	315 K	0.016	0
S(T)	2.4136×10 ⁻¹⁹ cm per molecule	0.9	39.8
x	1.987×10^{-6}	2.9	

4. Field Test of Mobile Monitoring for CH₄/C₂H₆ Leakage

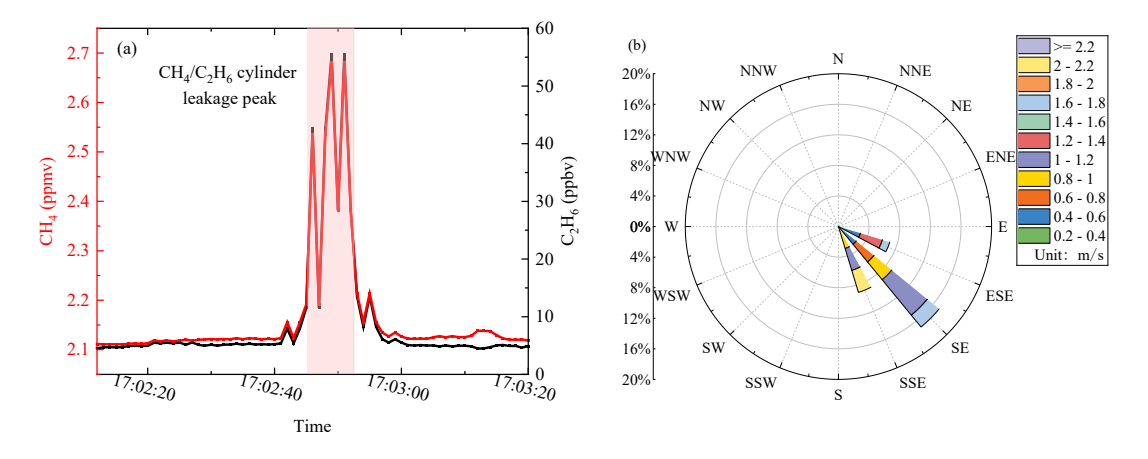
The vehicle-integrated platform is shown in Figure 6, including a front-mounted gas inlet with a particulate pre-filter for air sampling, a trunk-based CH_4/C_2H_6 sensor system for leak detection, and Roof-installed anemometer (DZZ20-UL, Janapo) and GPS module (UG-353, U-Blox) to monitor wind conditions and geolocation data. The photo shown in Figure 6 was captured at the simulated gas leakage experimental site on Zhenwu Road, Southeast University Science Park, on March 1, 2024. A gas mixture containing 1% CH_4 and 0.1% C_2H_6 (with N_2 as the balance gas) was used to simulate a natural gas leakage source. The geographic coordinates of the leakage source, obtained from AutoNavi Maps, were 31.88082° N, 118.81356° E. The shortest distance between this monitoring leakage point and the mobile monitoring vehicle was approximately 4 m. Appropriate institutional permission and risk clearance were obtained

prior to conducting the experimental testing in the University Science Park.



Figure 6. Field test of monitoring CH₄/C₂H₆ cylinder leakage at Zhenwu Road, Southeast University Science Park.

The gas leakage monitoring field experiment was conducted at an ambient temperature of approximately 21°C. A roof-mounted anemometer was deployed to measure wind speed and direction, while a GPS module recorded the vehicle's real-time trajectory and synchronized it with the map platform for visualization. As shown in Figure 7(c), the GPS module recorded the vehicle's position in real-time at a frequency of 1 Hz, while the on-board gas sensor simultaneously measured concentrations at the same rate. Combined with the vehicle's average speed of 20 km/h during normal operation, these synchronized datasets enabled the mapping of spatial gas concentration distribution through mobile monitoring. Figure 7(a) illustrates the gas concentration dynamics recorded during mobile monitoring, aligned with real-time positional updates. The maximum and minimum concentrations were 2.68 and 2.11 ppmv for CH₄, and 55.49 and 4.42 ppbv for C₂H₆. The background baseline values were approximately 2.1 ppmv and 4.5 ppbv for CH₄ and C₂H₆, respectively. As shown in Figure 7(b), the wind speed during the monitoring period ranged from approximately 0.4 to 2.1 m/s, with a mean value of 1.03 m/s. The prevailing wind direction was consistently Southeast, indicating stable atmospheric conditions. The thresholds of CH₄ and C₂H₆ for leak detection were set to the atmospheric background baseline values of 2.1 ppmv and 4.5 ppbv, respectively. The detection of natural gas leaks is driven by the CH₄/C₂H₆ concentration change in the leakage peak. When the correlation coefficient of the concentration variations between CH₄ and C₂H₆ is >0.8, and the leakage peaks of both gases exhibit a high correlation in concentration, the location can be identified as a high-probability gas leak suspect point.



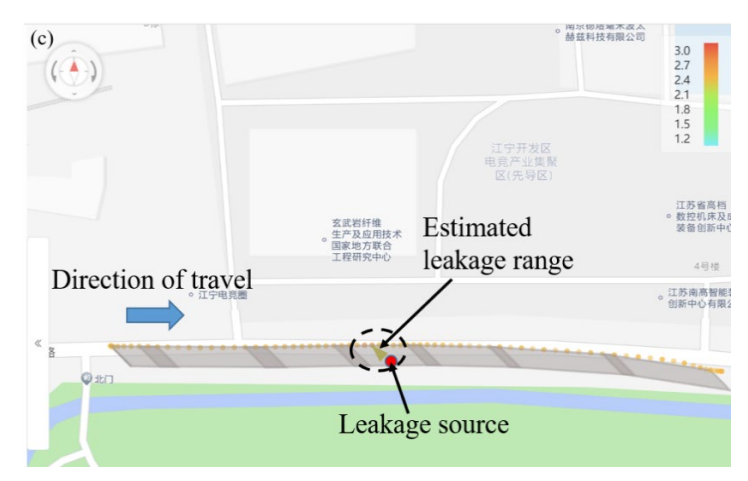


Figure 7 (a) Measured CH₄/C₂H₆ concentrations during in-vehicle mobile monitoring. (b) Wind-rose diagram. (c) Leakage source location and vehicle trajectory based on spatial distribution of measured concentrations.

The valve of the CH₄/C₂H₆ gas mixture cylinder was opened at 17:02:12 to initiate a controlled gas leak simulation. At the same time, the vehicle-integrated platform equipped with a CH₄/C₂H₆ gas sensor began traveling eastward along Zhenwu Road. At 17:02:45, the sensor detected the gas leak, triggering a rise in CH₄/C₂H₆ concentrations. The vehicle was positioned approximately 5 meters from the leakage source. The resulting plume persisted for approximately 9 s. The Pearson correlation coefficient between CH₄ and C₂H₆ concentrations at this time reached 0.9991, indicating nearly perfect synchrony in their fluctuations. This proportional co-dilution pattern during atmospheric dispersion strongly suggests a common leakage source. Through field testing, it was verified that genuine leakage manifests as synchronous concentration variations. Therefore, simultaneous monitoring of CH₄ and C₂H₆ concentrations enables reliable identification of natural gas leakage events. This approach establishes a diagnostic framework to differentiate pipeline leaks from other CH₄ sources through characteristic C₂H₆/CH₄ ratios, thereby enhancing urban gas distribution network surveillance. The mobile monitoring strategy incorporating this sensing system is expected to reduce methane leak duration to about 2 hours, which could result in a 90% reduction in emissions from a single point leak event. Taking a combined daily methane leakage volume of 710 m³ (from minor, moderate, and severe leaks) as an example, the annual average methane leakage volume can be reduced by about 230,000 m³, which is equivalent to a reduction of 4,611 tons of CO₂ equivalent. In terms of energy infrastructure safety, the system compresses the leak detection-to-repair time from 24 hours to 2 hours, which reduces the risk of gas explosion accidents and significantly enhances urban public safety by reducing this risk.

5. Conclusions

A dual-component gas sensor for CH₄ and C₂H₆ was developed based on a mid-infrared continuouswavelength interband cascade laser and a 13-m multi-pass gas cell. The sensor targets the CH₄ absorption lines at 2989.033 cm⁻¹, 2988.932 cm⁻¹, 2988.795 cm⁻¹, and the C₂H₆ absorption line at 2986.705 cm⁻¹. Operation under negative pressure (0.24 atm) was implemented to suppress water vapor interference, thereby enhancing the sensor's resistance to cross-sensitivity. Dynamic response testing of the sensor was conducted using CH₄ gas samples with varying volume fractions. The measured concentrations showed strong agreement with the prepared values, and the average response time was approximately 6 s. A long-term stability test was conducted using gas samples with 2 ppmv CH₄ and 1 ppmv C₂H₆. The measured average concentrations of CH₄ and C₂H₆ were 2.01 ppmv and 0.998 ppmv, with relative errors of 0.5% and 0.2%, respectively. Allan deviation analysis indicated that the MDL of CH₄ was 17.77 ppbv at an integration time of 1 s. When the integration time increased to 326 s, the MDL decreased to 1.19 ppbv. For C₂H₆, the MDL was 12.95 ppbv at 1 s and further reduced to 0.26 ppbv with an extended integration time of 393 s. Furthermore, field testing of mobile CH₄/C₂H₆ leakage monitoring demonstrated that a Pearson correlation coefficient of 0.9991 between the two gas concentrations near the leakage site enabled reliable differentiation of natural gas leaks from biological methane or other anthropogenic disturbances. The experimental results validated the sensor's high detection accuracy and long-term stability, aligning with the requirements for field applications in complex environments.

While the current study successfully validated the sensor's performance in a controlled leakage scenario, broader applicability requires further investigation into scalability and repeatability. The

modular design of the sensor system—comprising a tunable laser, compact multi-pass gas cell, and adaptable detection algorithms—lends itself to scalability. For instance, the optical path length and gas cell volume can be adjusted to accommodate varying detection ranges or environmental conditions, such as urban versus industrial settings. Additionally, the negative-pressure operation (0.24 atm) and temperature control mechanisms ensure stable performance across fluctuating humidity and temperature regimes, supporting repeatability in diverse climates. To enhance generalizability, future work will involve repeated experiments across multiple leakage scenarios, including varied leak rates, distances, and environmental backgrounds (e.g., high-traffic zones, residential areas). The system's real-time data processing framework and AI integration potential further enable rapid adaptation to dynamic conditions, ensuring reliable detection even in complex urban matrices. Field deployments across distributed gas networks, coupled with long-term stability assessments, will solidify its scalability for large-scale urban monitoring applications.

Future sensor development will focus on: miniaturization via micro-electromechanical systems and photonic integration for lightweight deployment (e.g., drones); enhanced extreme-environment resilience through corrosion-resistant materials and adaptive algorithms; AI-driven monitoring using dynamic C_2H_6 / CH_4 ratio analysis for leak identification; and IoT-based deployment strategies with low-power cellular networks and cloud data fusion for city-wide gas pipeline surveillance.

Acknowledgments

This research was supported by the Scientific and Technological Innovation Project of Carbon Emission Peak and Carbon Neutrality of Jiangsu Province (BE2023854 and BT2024013), the Fundamental Research Funds for the Central Universities (No.4003002506).

References

- M. Li, H. Zheng, X. Xue, et al., "Reliability evaluation and management of PetroChina's large-scale system of natural gas pipeline networks," *Journal of Natural Gas Geoscience*, vol. 4, no. 5, pp. 287–295, 2019, doi: 10.1016/j.jnggs.2019.07.003.
- S. Faramawy, T. Zaki, and A. A.-E. Sakr, "Natural gas origin, composition, and processing: A review," *Journal of Natural Gas Science and Engineering*, vol. 34, pp. 34–54, 2016, doi: 10.1016/j.jngse.2016.06.030.
- S. Halley, "Combined Mixed Potential Electrochemical Sensors and Artificial Neural Networks for the Quantification and Identification of Methane in Natural Gas Emissions Monitoring," *Journal of The Electrochemical Society*, vol. 168, pp. 097506, 2021, doi: 10.1149/1945-7111/ac2465.
- Y. Cho, K. M. Smits, S. N. Riddick, et al., "Calibration and field deployment of low-cost sensor network to monitor underground pipeline leakage," *Sensors and Actuators B: Chemical*, vol. 355, pp. 131276, 2022, doi: 10.1016/j.snb.2021.131276.
- S. Shelton, G. Liyanage, S. Jayasekara, et al., "Seasonal Variability of Air Pollutants and Their Relationships to Meteorological Parameters in an Urban Environment," *Advances in Meteorology*, vol. 2022, pp. 1–18, 2022, doi: 10.1155/2022/5628911.
- T. Rosli Razak, M. Hafiz Ismail, H. Jarimi, et al., "Machine Learning-Based Predictive Models for Indoor Air Quality and Thermal Comfort: Bridging Sensor Data and Human Perception in Healthcare Facilities," *Energy Catalyst*, vol. 1, pp. 35–53, 2025, doi: 10.61552/ec.2025.003.
- M. Barriault, I. Alexander, N. Tasnim, et al., "Classification and Regression of Binary Hydrocarbon Mixtures using Single Metal Oxide Semiconductor Sensor with Application to Natural Gas Detection," *Sensors and Actuators B: Chemical*, vol. 326, pp. 129012, 2021, doi: 10.1016/j.snb.2020.129012.
- G. Menduni, A. Zifarelli, A. Sampaolo, et al., "High-concentration methane and ethane QEPAS detection employing partial least squares regression to filter out energy relaxation dependence on gas matrix composition," *Photoacoustics*, vol. 26, pp. 100349, 2022, doi: 10.1016/j.pacs.2022.100349.
- T. Aldhafeeri, M.-K. Tran, R. Vrolyk, et al., "A Review of Methane Gas Detection Sensors: Recent Developments and Future Perspectives," *Inventions*, vol. 5, no. 3, pp. 28, 2020, doi: 10.3390/inventions5030028.
- B. Jeevaretanam, M. Abuseada, C. Wei, et al., "Transient analysis of solar pyrolysis and hydrogen yield via interband cascade laser absorption spectroscopy of methane, acetylene, ethylene, and ethane," *Applications in Energy and Combustion Science*, vol. 16, pp. 100223, 2023, doi: 10.1016/j.jaecs.2023.100223.
- N. M. Davis, D. Francis, J. Hodgkinson, et al., "Compact methane sensor using an integrating sphere and interband cascade laser at 3313 nm," *Sensors and Actuators B: Chemical*, vol. 389, pp. 133866, 2023, doi: 10.1016/j.snb.2023.133866.
- L. E. Mchale, B. Martinez, T. W. Miller, et al., "Open-path cavity ring-down methane sensor for mobile monitoring of natural gas emissions," *Optics Express*, vol. 27, no. 14, pp. 20084–20097, 2019, doi: 10.1364/OE.27.020084.
- A. Sampaolo, S. Csutak, P. Patimisco, et al., "Methane, ethane and propane detection using a compact quartz enhanced photoacoustic sensor and a single interband cascade laser," *Sensors and Actuators B: Chemical*, vol. 282, pp. 952–960, 2019, doi: 10.1016/j.snb.2018.11.132.

- C. Floridia, J. B. Rosolem, J. P.-V. Fracarolli, et al., "Evaluation of Environmental Influences on a Multi-Point Optical Fiber Methane Leak Monitoring System," *Remote Sensing*, vol. 11, no. 10, pp. 1249, 2019, doi: 10.3390/rs11101249.
- M. Zou, L. Sun, X. Wang, "CH₄/C₂H₆ dual-gas sensing system based on wavelength modulation spectroscopy using a single near infrared laser," *Spectrochimica Acta Part A: Molecular and Biomolecular Spectroscopy*, vol. 272, pp. 120970, 2022, doi: 10.1016/j.saa.2022.120970.
- A. Zifarelli, A. Sampaolo, P. Patimisco, et al., "Methane and ethane detection from natural gas level down to trace concentrations using a compact mid-IR LITES sensor based on univariate calibration," *Photoacoustics*, vol. 29, pp. 100448, 2023, doi: 10.1016/j.pacs.2023.100448.
- I. E. Gordon, L. S. Rothman, R. J. Hargreaves, et al., "The HITRAN2020 molecular spectroscopic database," *Journal of Quantitative Spectroscopy and Radiative Transfer*, vol. 277, pp. 107949, 2022, doi: 10.1016/j.jqsrt.2021.107949.